

1  
2 **Prediction of DNA i-Motifs Via Machine Learning**  
3

4 Bibo Yang,<sup>1,†</sup> Dilek Guneri,<sup>2,†</sup> Haopeng Yu,<sup>1,†,\*</sup> Elisé P. Wright,<sup>3</sup> Wenqian Chen,<sup>2</sup> Zoë A. E. Waller,<sup>2</sup>  
5 \* Yiliang Ding<sup>1,\*</sup>

6  
7 <sup>1</sup> Department of Cell and Developmental Biology, John Innes Centre, Norwich Research Park,  
8 Norwich, NR4 7UH, UK

9 <sup>2</sup> School of Pharmacy, University College London, London, WC1N 1AX, UK

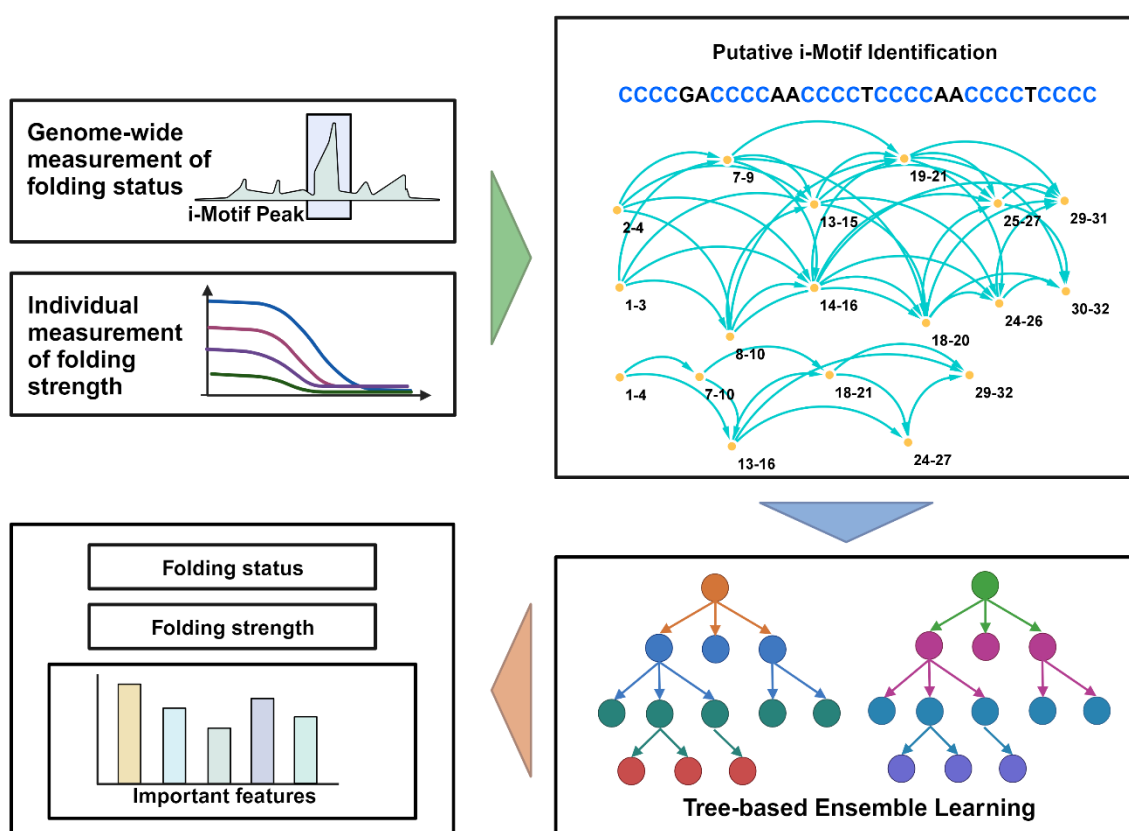
10 <sup>3</sup> Molecular Physiology School of Medicine, and Molecular Medicine Research Group, University  
11 of Western Sydney, Campbelltown, NSW 1797, Australia

12 \*To whom correspondence should be addressed. Tel: +44 (0)1603 450266; Email:  
13 yiliang.ding@jic.ac.uk. Correspondence may also be addressed to [haopeng.yu@jic.ac.uk](mailto:haopeng.yu@jic.ac.uk) or  
14 [z.waller@ucl.ac.uk](mailto:z.waller@ucl.ac.uk).

15 <sup>†</sup>Joint First Authors.

16

17 **GRAPHICAL ABSTRACT**



18

19 **ABSTRACT**

20 i-Motifs (iMs), are secondary structures formed in cytosine-rich DNA sequences and are  
21 involved in multiple functions in the genome. Although putative iM forming sequences are

22 widely distributed in the human genome, the folding status and strength of putative iMs vary  
23 dramatically. Much previous research on iM has focused on assessing the iM folding properties  
24 using biophysical experiments. However, there are no dedicated computational tools for  
25 predicting the folding status and strength of iM structures. Here, we introduce a machine  
26 learning pipeline, iM-Seeker, to predict both folding status and structural stability of DNA iMs.  
27 The programme iM-Seeker incorporates a Balanced Random Forest classifier trained on  
28 genome-wide iMab antibody-based CUT&Tag sequencing data to predict the folding status  
29 and an Extreme Gradient Boosting regressor to estimate the folding strength according to  
30 both literature biophysical data and our in-house biophysical experiments. iM-Seeker predicts  
31 DNA iM folding status with a classification accuracy of 81% and estimates the folding strength  
32 with coefficient of determination ( $R^2$ ) of 0.642 on the test set. Model interpretation confirms  
33 that the nucleotide composition of the C-rich sequence significantly affects iM stability, with a  
34 positive correlation with sequences containing cytosine and thymine and a negative  
35 correlation with guanine and adenine.

36

## 37 INTRODUCTION

38 Nucleotides are the basic units that form DNA and RNA, two key molecules in the central  
39 dogma. DNA encodes genetic information, which is transcribed to mRNA and then translated  
40 to protein. In addition to this transfer of information, DNA and RNA can form complex  
41 structures, which can play crucial functional roles in organisms. Besides the canonical Watson-  
42 Crick double-helical B-form structure, DNA can form non-canonical secondary structures such  
43 as G-quadruplexes (G4s) and i-Motifs (iMs). G4s are four-stranded structures formed from G-  
44 rich sequences and are stabilised by Hoogsteen hydrogen bonding between guanines (1). iMs  
45 are also four-stranded structures, but formed from cytosine C-rich regions that are stabilised  
46 by hemi-protonated C-C base pairs ( $C^+:C$ ) (2,3). Complementary G-rich and C-rich sequences  
47 can form G4s and iMs interdependently during distinct cellular processes (4). As a non-  
48 canonical structure, iMs are indicated to play an important role in the genome. There are an  
49 increasing number of *in vitro* and *in cellulo* studies that report evidence that iMs could fold in  
50 promotor region of certain genes, telomeres and untranslated regions. They have also been  
51 implicated as a regulatory element associated with the cell cycle, transcription, chromatin  
52 remodelling, as well as transposable element dynamics (5-7).

53 Commonly, computational analysis of putative iMs is limited to indirect identification by  
54 searching for potential complementary G4 sequences in the genome (8). Plenty of G4  
55 prediction tools have been developed previously, and these can generally be divided into two  
56 categories based on whether or not the models utilised experimentally-derived G4-specific  
57 data. Classical computational tools which do not use G4-specific data, are typically constructed  
58 from string-matching models based on a specific sequence pattern. Others use a designed  
59 scoring system according to pre-defined rules. For example, platforms like Quadparser (9),  
60 Quadruplexes (10), and AllQuads (11), used algorithms like regular expression to search  
61 G4 forming sequences, whilst QGRS Mapper (12), G4P (13), and G4hunter (14), use scoring  
62 models that can estimate the probability or strength of putative G4s (15). These models  
63 have potential to be used in iM-forming sequences searching, because the putative iMs have  
64 in principle similar sequence patterns and some of the rules will be transferrable to both  
65 structures. For example, enrichment of G/C in a C/G-rich sequence disfavours both G4 and iMs.  
66 In contrast, there are also platforms guided by G4-specific data (e.g., biophysical properties,  
67 G4 ChIP-seq, G4 CUT&Tag, and G4-seq) that can capture additional G4-specific features to  
68 improve the G4 prediction performance (16). Software like PQSfinder (17), G4boost (18),  
69 Quadron (19), DeepG4 (20), and G4-folding energy estimation module integrated in RNAFold  
70 (21) use data from G4-specific experiments to increase the accuracy of predictions. Therefore,  
71 the application of these models on iM identification is limited. Out of the existing searching  
72 platforms, G4-Hunter is the easiest to use for searching for iMs as it was designed to take into  
73 account C with negative values both to disfavour regions rich in alternative G/C and to score  
74 both strand of a DNA duplex simultaneously. C-richness and C-skew is obviously important  
75 for iM formation (14). Besides, G4-iM Grinder can also be used to predict and evaluate G4 and  
76 iM forming sequences (22). Typically, individual C-rich sequences are biophysically assed for  
77 their capability to form iMs. UV spectroscopy is typically used to determine the thermodynamic  
78 properties such as melting ( $T_m$ ) and annealing ( $T_a$ ) temperatures (23). Furthermore, thermal  
79 difference spectra (TDS) are typically generated, using the difference in absorbance spectra  
80 between folded and unfolded DNA, determining a signature to identify the formed secondary  
81 DNA structure (24). UV spectroscopy is often accompanied with circular dichroism (CD)  
82 spectroscopy to conform the formation of i-motif structure. The transitional pH ( $pH_T$ ) is an

83 important measure of the stability of iM structures, determined by assessing the formation of  
84 iM across a pH-range (8,25-27).

85 A systematic prediction tool to identify DNA iM folding status and their potential  
86 stability is lacking. Recently, the landscape of iM forming sequences in the whole human  
87 genome was determined via the novel CUT&Tag sequencing using anti-iM iMab antibodies on  
88 living human cells (7). Here we introduce, iM-Seeker, a novel computational pipeline using the  
89 genome-wide iM profile (7), iM-stability data from the literature, and our in-house biophysical  
90 analysis to predict iM structure formation and stability. iM-Seeker utilised a newly-designed  
91 graph-based algorithm to search for putative iM forming sequences within an entered DNA  
92 sequence. The Balanced Random Forest script is trained on the iMs identified in the human  
93 genome derived from iMab-based CUT&Tag sequencing data (7) and was further developed  
94 to predict iM structure folding status within DNA sequences. iM-Seeker also incorporates the  
95 Extreme Gradient Boosting (XGBoost) regressor to predict the structure stability, by cross  
96 referencing iM forming DNA sequences to their corresponding pH<sub>T</sub> values. Furthermore, this  
97 computational model has shed new insight into the importance of nucleotide composition in  
98 iM stability. A positive correlation was observed for sequences containing cytosine and  
99 thymine whilst sequences rich in guanine and adenine were found to have a negative  
100 correlation with iM stability. Alongside nucleotide composition, long C-tract lengths  
101 accompanied with short loop lengths contribute towards high stability of iM structure.

102

## 103 MATERIAL AND METHODS

### 104 Data collection

105 We collected the published CUT&Tag sequencing data in the human genome (7). The data was  
106 downloaded from the NCBI GEO database (accession number GSE220882). The BigWig format  
107 data included iM forming sequences from both 93T449 (WDLPS) cell line and human  
108 embryonic kidney (HEK293T) cell line with three biological replicates for each cell line. The  
109 focus was concentrated on HEK293T cell data which was presented with more high-confident  
110 iM regions than WDLPS cells (7). The downloaded BigWig files were converted to bedGraph  
111 files and iM-peak region were cumulated with SEACR v1.3 set to "0.01 non stringent"

112 parameters (7,28). The intersected iM-peak regions among three biological replicates were  
113 defined as the final high-confident iM-peak regions. Literature-derived data of i-Motif forming  
114 sequences and their corresponding pH<sub>T</sub> values were collected (Supplementary Table S1).

115

## 116 **Graph-based putative i-motif searching**

117 Putative i-Motifs can be identified based on their sequence pattern (C<sub>≥3</sub>N<sub>1-12</sub>)<sub>3</sub>C<sub>≥3</sub> where C  
118 represents cytosine and N represent any nucleotide (29,30). The classic approach to identify  
119 potential putative iM-forming sequences is to search complementary sequences of G4-  
120 forming sequences based on sequence pattern matching. This assumption and current  
121 approaches limit the identification of iMs with their different variations in C:C(+) formations  
122 and topologies compared to G4s (29,30). To overcome this limitation, we designed a general  
123 pattern for iM formation searching using directed graph traversal process. For one sequence,  
124 the C-tracts can be regarded as nodes, and the loops can be defined as edges. All possible C-  
125 tracts (C-tract length  $\geq 3$ ) are identified as nodes in the first phase, and if the distance between  
126 two nodes (loop length) is between one and twelve nucleotides, a directed edge is added  
127 between the two nodes. After constructing the directed graph, all possible iM formations and  
128 conformations are identified via the traversal of the directed graph from every node. All  
129 possible putative iMs are represented with the sub-population containing the first four nodes  
130 and three edges of the traversing paths with at least four nodes. To choose the representative  
131 iM structures from all possible iM structures, four strategies were introduced (greedy non-  
132 overlapping, greedy overlapping, non-greedy non-overlapping, and non-greedy overlapping)  
133 maintaining the nomenclature derived from QuadBase2 (31). Overlapping strategy selects an  
134 iM representative structure for each iM starting coordinate while the non-overlapping function  
135 has no coinciding iM representatives. The greedy strategy maximises the loop length of iM  
136 representatives with longest C-tract. For non-greedy strategies, the iM with the most extended  
137 C-tract length and the shortest loop length can be selected. One representative iM forming  
138 sequence may have many different iM conformations although they share the same sequence  
139 content. Two representative iM formations are chosen for according to their stability: (A) the  
140 structure with minimum standard deviation of loop lengths; (B) the structure with minimum  
141 length of the two side loops. We called the initial computational pipeline Putative-iM-Searcher  
142 (Figure 1A).

143

#### 144 **Dataset construction and feature selection for machine learning**

145 We employed a Putative-iM-Searcher in high-confident iM-peak regions and interval regions  
146 in both Watson and Crick strands in the human reference genome (GRCh38). Putative iMs in  
147 high confident iM-peak regions were defined as folded iMs, and unfolded C-rich sequences in  
148 interval regions. We used a non-overlapping strategy to avoid bias in the performance  
149 estimation of the classification model. Four classification datasets were constructed:  
150 (Classification dataset 1) non-overlapping, greedy and conformation A; (Classification dataset  
151 2) non-overlapping, greedy and conformation B; (Classification dataset 3) non-overlapping,  
152 non-greedy and conformation A; (Classification dataset 4) non-overlapping, non-greedy and  
153 conformation B.

154

155 We selected the data items with reliable  $pH_T$  from literature-derived data. We also generated  
156 our in-house biophysical experimental data for developing regression models. The Putative-  
157 iM-Searcher was applied to filtered dataset of iM forming sequences with their corresponding  
158  $pH_T$  values. The iMs which meet the sequence pattern with corresponding  $pH_T$  were used for  
159 regression model construction. We also filtered iM items with the same putative iM forming  
160 sequence but different  $pH_T$  and combined iM items with the same putative iM forming  
161 sequence and  $pH_T$  to avoid bias. Both our classification model and regression model used  
162 thirty-three different features: C-tract length, iM length, loop length, middle loop length,  
163 longest side loop length, shortest side loop length, sum of two side loops, longest loop length,  
164 shortest loop length, A density in iMs, C density in iMs, G density in iMs, T density in iMs, A  
165 density in loops, C density in loops, G density in loops, T density in loops, A density in middle  
166 loop, C density in middle loop, G density in middle loop, T density in middle loop, A density in  
167 longest side loop, C density in longest side loop, G density in longest side loop, T density in  
168 longest side loop, A density in shortest side loop, C density in shortest side loop, G density in  
169 shortest side loop, T density in shortest side loop, A density in two side loops, C density in two  
170 side loops, G density in two side loops, T density in two side loops. For the regression system,  
171 the iM folding strength is defined as the  $pH_T$  after standardization and min-max scaling.

172

173 **The imbalanced ensemble learning to predict folded and unfolded i-motifs**

174 A five-fold cross-validation assessment was applied to evaluate the classification performance  
175 of the iMs for four datasets via nine classifiers including Decision Trees (32), Random Forest  
176 (33), Balanced Random Forest (34), Naive Bayes (35), Linear Discriminant Analysis (36), Easy  
177 Ensemble (37), Balanced Bagging (38,39), Random Undersampling Boosting (RUSBoost) (40),  
178 and Extreme Gradient Boosting (XGBoost) algorithms (41). The combination of dataset and  
179 model which achieve best performance via area under the receiver operating characteristic  
180 curve (AUROC) and balanced accuracy, was used for classification. 90% of data in the whole  
181 dataset was randomly selected and separated into a training & validation set, and the  
182 remaining 10% of data was used as the test set. Five-fold cross-validation and grid searching  
183 on training & validation set were employed to search for the best hyperparameters and test  
184 set was used to evaluate the model's classification performance on accuracy, recall, specificity,  
185 and AUROC.

186

187 **The regression algorithm to measure the strength of i-motif using ensemble learning.**

188 Consistent iM searching and conformation identification strategy with classification dataset  
189 was applied in the regression model. A five-fold cross validation assessment was applied to  
190 evaluate the regression performance of the iMs based on thirteen regressors including  
191 Decision Trees (32), Random Forest (33), Linear Regression (42), Ridge Regression (43), Lasso  
192 Regression (44), Elastic Net Linear Regression (45), Linear Support Vector Regression (46),  
193 Radial Basis Function Support Vector Regression (47), K-Nearest Neighbors Regression (KNN)  
194 (48), Adaptive Boosting (AdaBoost) (49), Gradient Boosting (50), Extreme Gradient Boosting  
195 (XGBoost) (41), and Random Sample Consensus (RANSAC) algorithms (51). 80% of data in the  
196 whole dataset was separated into training & validation set randomly for hyperparameters  
197 adjustment by five-fold cross-validation and grid searching, and 20% of data was used to  
198 evaluate the regression performance of the model by coefficient of determination ( $R^2$ ), root  
199 mean squared error (RMSE), and mean absolute error (MAE) (18). The feature importance of  
200 the regression model was extracted from the model with 'importance\_type=gain'.

201

202 **Implementation**

203 The algorithm was written in Python 3, and machine learning was employed via the Python  
204 Scikit-learn package (52), Imbalanced-learn package (53), and XGBoost package (41). The  
205 source code and documentation of Putative-iM-Searcher are available at  
206 <https://github.com/YANGB1/Putative-iM-Searcher>. Combining the classification model and  
207 regression model, we built a computational tool called iM-Seeker, which is available at  
208 <https://github.com/YANGB1/iM-Seeker>.

209

## 210 **Biophysical Characterisation of C-rich DNA sequences**

211 The test oligonucleotides were synthesised and reverse phase HPLC purified by Eurogentec  
212 (Belgium) and were resuspended in ultra-pure water. The DNA final concentration was  
213 confirmed via Nanodrop. Samples were prepared as 10  $\mu$ M DNA in 10 mM sodium cacodylate  
214 (NaCaco) and 100 mM KCl buffer with the range of pH 4-8. The DNA samples were annealed  
215 prior to biophysical characterisation by denaturing the DNA for 5 mins at 95°C and allowing  
216 to reanneal by slowly cooling down to room temperature, overnight.

217 The CD spectra of the annealed C-rich sequences were recorded on a JASCO 1500  
218 spectropolarimeter under a constant flow of nitrogen. An accumulation of four CD spectra  
219 scans was acquired from 200-320 nm at 20°C with a data pitch of 0.5 nm, scanning speed of  
220 200 nm/min with 1 second response time, 1 nm bandwidth, and 200 mdeg sensitivity. The  
221 measured DNA samples and buffer at corresponding pH were subtracted before zero  
222 correction at 320 nm. The transitional pH ( $pH_T$ ) was determined by plotting the measured  
223 ellipticity at 288 nm and pH range and the resulting inflection point of the Boltzmann  
224 sigmoidal or bi-phase sigmoidal fit using Graphpad Prism (Version 10.1.0.316).

225 The CD samples at pH 5.5 were diluted in the same buffer to 2.5  $\mu$ M final DNA  
226 concentration. These samples were used to perform UV spectroscopy to obtain the thermal  
227 difference spectra (TDS) and determine the melting temperature ( $T_M$ ), annealing temperature  
228 ( $T_A$ ) and their respective hysteresis ( $T_H$ ). For melting/annealing experiments, the absorbance at  
229 295 nm was measured at every 1°C increase/decrease in three cycles of denaturation and  
230 reannealing. The cycle begins with 10 mins at 4°C followed by gradual increase of 0.5°C/min  
231 to 95°C (melting). Once the final temperature was reached, the samples were kept at 95°C for  
232 10 mins before reversing the process (annealing). The melting and annealing temperatures  
233 were determined via the first derivative method of for each measured cycle as previously

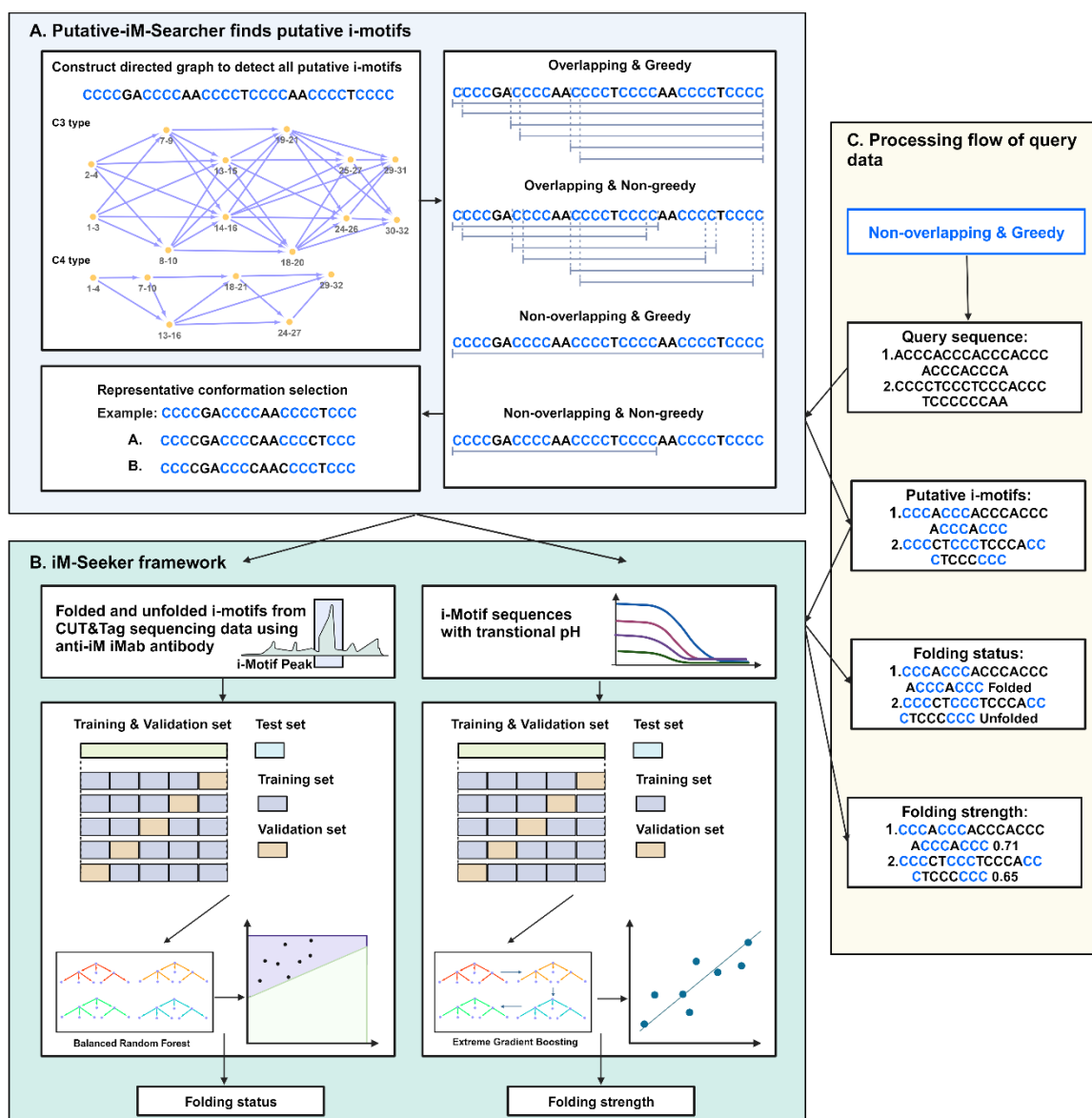
234 described (54). The samples were kept at 4°C after the completion of the final reannealing  
235 cycle. For the thermal difference spectra (TDS), these samples were used to obtain the  
236 absorbance spectrum (230-320 nm). The samples were kept at 4°C for an additional 10 mins  
237 before measuring the absorbance spectrum of potentially folded iMs. This was followed by a  
238 second absorbance spectrum after 10 mins at 95°C for the unstructured DNA structure.  
239 Individual TDS signatures were determined by subtracting both absorbance spectra (unfolded-  
240 folded DNA structure), zero correcting at 320 nm, and finally normalisation to the maximum  
241 absorbance to 1 as previously described (24).

242

243 **RESULTS**

244 **Description of the iM-Seeker framework**

245 iM-Seeker is a computational framework using machine learning to predict the folding status  
246 and folding strength of iMs. The outline of the whole iM-Seeker structure is shown in Figure  
247 1. The Putative-iM-Searcher was developed to discover the putative iM forming sequences  
248 (Figure 1A). Putative-iM-Searcher constructs a directed graph model and obtains  
249 representative conformation from all DNA structure conformations based on the configuration  
250 of overlapping & non-overlapping strategy, greedy & non-greedy strategy, and  
251 representative-conformation-selection strategy. The Balanced Random Forest classification  
252 model and XGBoost regression model were trained on iMab-based genome-wide iM  
253 landscape and biophysical experimental justified iM with pH<sub>T</sub>, respectively, for the folding  
254 status prediction and folding strength estimation (Figure 1B). The workflow of iM-Seeker after  
255 receiving the query sequences is shown in Figure 1C. Putative-iM-Searcher was applied to  
256 query sequences to find putative iM forming sequences in the first stage. For each putative iM  
257 individual, the Balanced Random Forest classification model will be used to predict the folding  
258 status. Next, an estimated folding strength score was calculated by the XGBoost regression  
259 model for putative iM individuals.



260

261 **Figure 1.** The outline of the whole iM-Seeker. **(A)** The framework of Putative-iM-Searcher. Putative-iM-  
262 Searcher can detect all i-motif conformation and representative conformation based on overlapping &  
263 non-overlapping strategy, greedy & non-greedy strategy, and representative-conformation strategy. **(B)**  
264 The framework of iM-Seeker. iM-Seeker employs Putative-iM-Searcher to find putative i-motif forming  
265 sequences. Balanced Random Forest classification model and XGBoost regression model are developed  
266 to predict the folding status and folding strength, respectively. **(C)** The processing flow of query data  
267 using iM-Seeker. Created with BioRender.com.

268

269 **iM-Seeker predicts iM structure folding status**

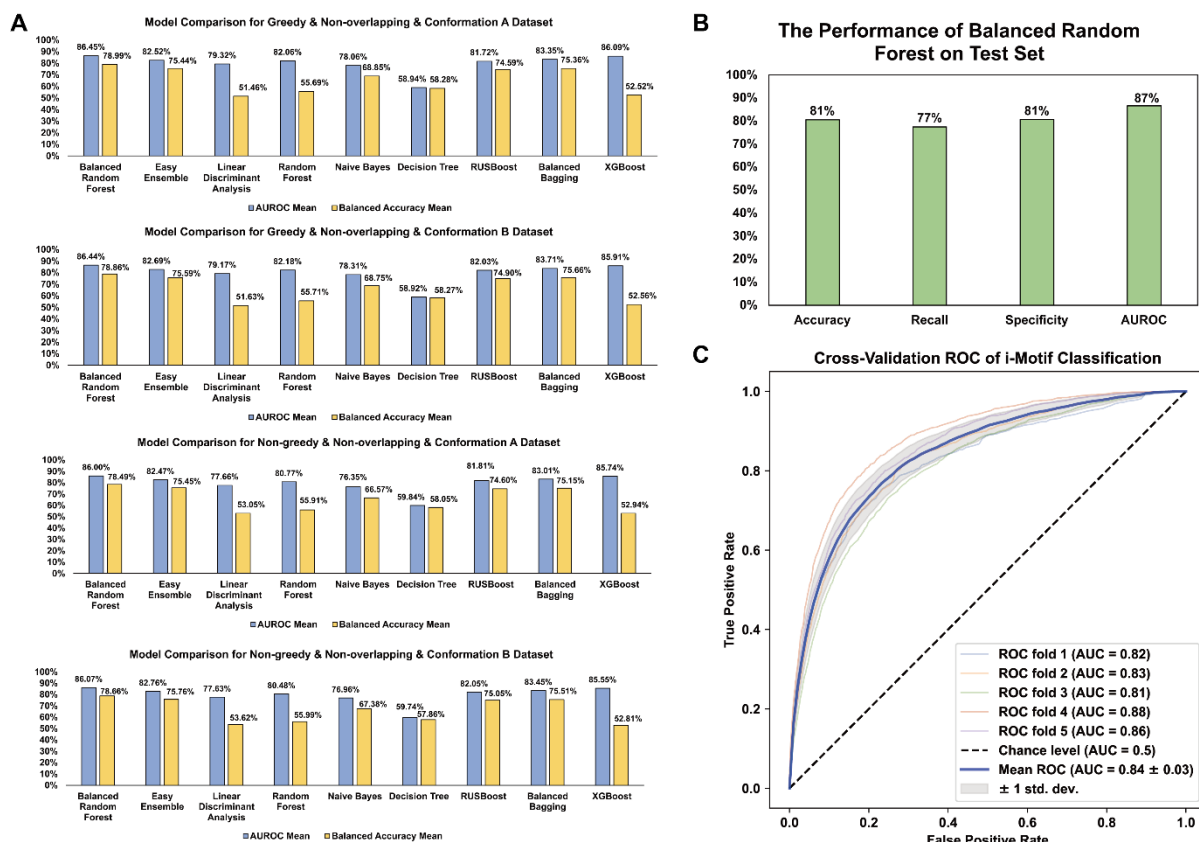
270 Putative iM forming sequences in the intersected high-confident iM-peak regions among  
271 three biological replicates from the CUT&Tag sequencing data were defined as folded iMs  
272 while unfolded C-rich sequences can be found in interval regions. For greedy and non-  
273 overlapped two classification datasets, they both included 8,837 folded iMs and 733,115  
274 unfolded C-rich sequences while 9,641 folded iMs and 755,747 unfolded C-rich sequences  
275 were in non-greedy and non-overlapped two datasets.

276

277 Thirty-three features from labelled folded and unfolded putative iM sequences were derived.  
278 A five-fold cross-validation assessment was applied on nine classifiers on four classification  
279 datasets to select the best dataset and model. Considering the mean AUROC score and mean  
280 balanced accuracy of five folds, Balanced Random Forest performed best in all four datasets  
281 because the balanced learning strategy can better fit our imbalanced datasets. Thus, Balanced  
282 Random Forest was selected as the final classifier. Greedy and non-overlapped two datasets  
283 outperformed the non-greedy and non-overlapped datasets in terms of the two indicators.  
284 Although there is no significant difference between conformation A and B for greedy and non-  
285 overlapped datasets, both AUROC and balanced accuracy of conformation A were found to be  
286 higher than B (Figure 2A). Thus, we chose conformation A dataset of greedy and non-  
287 overlapped strategy as final dataset for classification task.

288

289 The whole dataset was divided into the training & validation set (90%) and test set (10%)  
290 because the whole dataset contains ~740,000 data items, test set with ~74,000 (10%) data  
291 items is enough to test the model performance. The Balanced Random Forest model was  
292 optimised by cross-validation and grid search on training & validation set. We evaluated the  
293 model performance on the test set with 81% accuracy, 77% recall, 81% specificity, and 87%  
294 AUROC score, which show the model can achieve good performance in both folded iMs and  
295 unfolded C-rich sequences (Figure 2B). Besides, we assessed the model's generalisation  
296 performance through five-fold cross-validation deployed across the entire dataset on AUROC  
297 (Figure 2C). The AUROC scores on all five folds are all higher than 0.8, which shows the excellent  
298 generalisation performance.



299

300 **Figure 2.** Model selection and performance estimation of classification model. **(A)** The comparison  
301 among nine models (Decision Trees, Random Forest, Balanced Random Forest, Naive Bayes, Linear  
302 Discriminant Analysis, Easy Ensemble, Balanced Bagging, RUSBoost, and XGBoost) on four classification  
303 datasets. AUROC and balanced accuracy show that Balanced Random Forest on greedy & non-  
304 overlapping & conformation B dataset has the best performance. **(B)** The performance of Balanced  
305 Random Forest classifier on the test set. Accuracy, recall, specificity, and AUROC can reach 81%, 77%,  
306 81%, and 87% respectively. **(C)** The ROC curves for classification performance. The Receiver Operating  
307 Characteristic (ROC) for the five-fold cross validation is shown. Each fold coloured separately with the  
308 AUC score and the mean ROC curve are coloured blue, and the random probability is shown as black  
309 dash lines.

### 310 **iM-Seeker measures the iM structure stability**

311 The literature-derived data (Supplementary Table S1) and the experimental biophysical data  
312 (Supplementary Table S2) were combined to a collection of 206 C-rich DNA sequences with  
313 their corresponding pH<sub>T</sub> values. The comparison of CD spectroscopy, UV spectroscopy, and  
314 TDS between representative iM forming sequence and representative non-iM forming  
315 sequence shows the reliability of our experiments (Supplementary Figure S1). However, one  
316 study contained 196 different sequences which contained only C and T. To avoid bias, these

317 DNA sequences were excluded to avoid misinterpretation of the importance of different  
318 nucleotides in the loops. 171 data items were selected as high-confident iM-containing items  
319 from 206 items based on criteria including TDS (Supplementary Data Set 1). After filtering data  
320 items with the same putative iM but different pH<sub>T</sub> and combining iM items with the same  
321 putative iM and equal pH<sub>T</sub> from high-confident data items, 120 putative iMs were extracted  
322 from the remaining sequence segments using the consistent Putative-iM-Searcher strategies  
323 (greedy, non-overlapped, and conformation A) with classification session followed by feature  
324 selection (Supplementary Data Set 2). The 120 pH<sub>T</sub> values standardized and rescaled to range  
325 from 0 to 1 via min-max scaling to define iM folding stability.

326

327 A five-fold cross-validation assessment was applied to thirteen regressors on regression  
328 datasets to find the model. Considering the mean of three indicators ( $R^2$ , RMSE, and MAE) on  
329 five-folds, XGBoost was selected as the final model because of the best performance (Table 1).  
330 The whole dataset was divided into training & validation set with 80% data and test set  
331 containing the remaining data. After optimization using cross-validation and grid search on  
332 training & validation set, the final XGBoost model was applied to the test set to assess the  
333 performance.  $R^2$ , RMSE, and MAE can reach 0.642, 0.104, and 0.08, respectively, which shows  
334 the model can achieve good performance in estimating the folding strength (Figure 3). The  
335 Pearson Correlation Coefficient (PCC) also reveals a strong correlation between measured and  
336 predicted folding strength ( $p < 10^{-7}$ ).

337

338

339

340

341

342

343

344

345

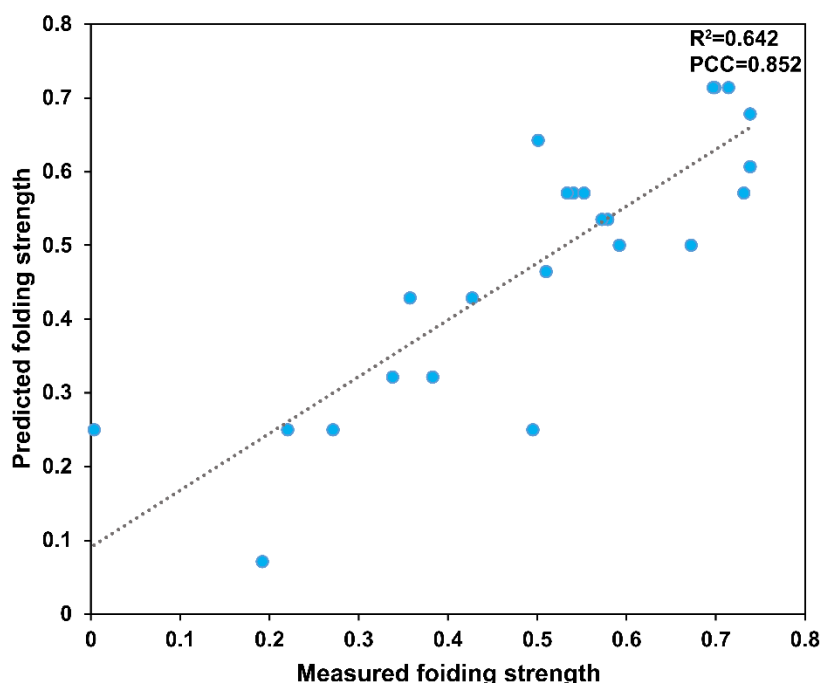
346

347

348 **Table 1.** Model comparison of thirteen regressors.

<b>Index</b>	<b>R<sup>2</sup> Mean</b>	<b>Root Mean Squared</b>	<b>Mean Absolute Error</b>
		<b>Error Mean</b>	<b>Mean</b>
Linear Regression	-0.158	0.195	0.139
Ridge Regression	-0.012	0.182	0.132
Lasso Regression	-0.027	0.185	0.146
Elastic Net Linear Regression	-0.027	0.185	0.146
Decision Tree	-0.002	0.181	0.134
Random Forest	0.434	0.138	0.105
Support Vector Regression	-0.043	0.185	0.130
Radial Basis Function			
Support Vector Regression	0.187	0.165	0.120
KNN	0.111	0.173	0.128
AdaBoosting	0.355	0.147	0.113
Gradient Boosting	0.379	0.144	0.110
RANSAC	-2.184	0.315	0.222
XGBoost	0.458	0.134	0.103

349



350

351 **Figure 3.** The performance evaluation of the XGBoost regressor on the test set (n=24). The Pearson  
352 Correlation Coefficient (PCC, 0.852,  $p < 10^{-7}$ ) and  $R^2$  (0.642) show a positive correlation between  
353 measured and predicted iM folding strength.

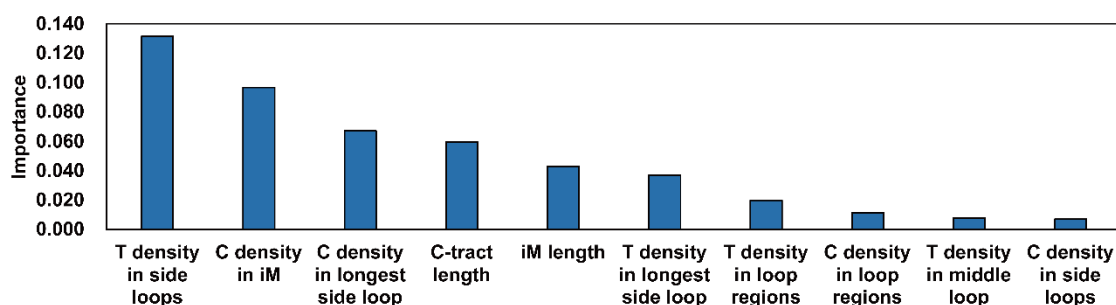
354

### 355 **Model interpretation provides insights into important features for iM stability**

356 We investigated the relative importance of the iM features extracted from the regression model.  
357 Features with high importance contribute more to the construction of the model and may play a more  
358 crucial role in iM formation than features with low importance. We divided the features into two groups  
359 based on the Pearson Correlation Coefficient (PCC): features with positive PCC were assumed to  
360 strengthen iM formation (Supplementary Table S3). In contrast, negative-correlated features were  
361 supposed to have a negative effect (Supplementary Table S4). In each group, the top 10 critical features  
362 are shown in Figure 4. Nucleotide composition affects the stability of iM structures. Stable iMs prefer to  
363 contain more C and T, especially T in side loops (Figure 4A). High G density and A density are associated  
364 with unstable iMs, especially these two nucleotides in side loops (Figure 4B). In addition, the C-tract  
365 length and loop length are two dominant features in all length-relative features. Long C-tract and short  
366 loop length can help with iM stability. Previous studies showed that in the same experimental condition,  
367 iMs with long C-tracts tend to be more stable than iMs with short C-tracts (55,56).

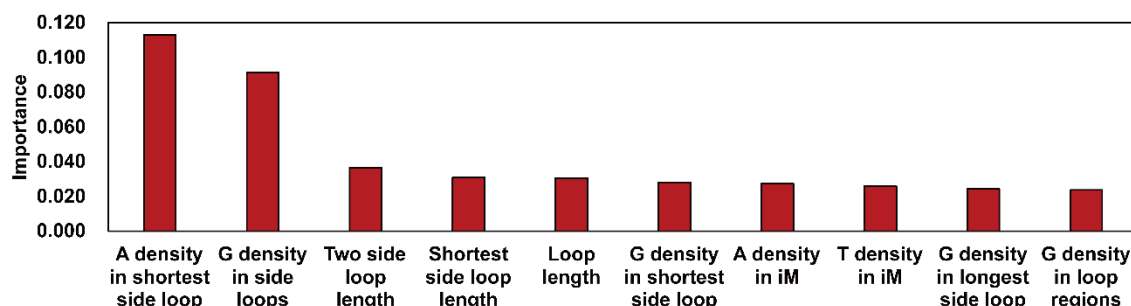
A

Top 10 important features with positive PCC with folding strength



B

Top 10 important features with negative PCC with folding strength



368

369 **Figure 4.** The iM feature importance obtained from the regression model. (A) Top 10 important features  
370 with positive Pearson Correlation Coefficient (PCC) with folding stability. (B) Top 10 important features  
371 with negative Pearson Correlation Coefficient (PCC) with folding stability.

372

## 373 DISCUSSION

374 Unlike the computational prediction of G4 structures, iMs are more complex in terms of what  
375 makes them stable (8,27,29,57-60) and it has been difficult to make predictions about iMs in  
376 the same way as G4s. Although, putative iMs have a similar sequence pattern to G4s, the  
377 stability of the structures has been more difficult to predict, as it has been shown that iMs can  
378 tolerate changes in sequence more than G4s (29), but are overall less stable in general.  
379 Therefore, iM-specific experimental data is critical to construct accurate computational models  
380 for iM prediction and stability. To the best of our knowledge, there are no iM-specific  
381 computational tools. Due to the similarity in sequence patterns between G4 and iM, some  
382 previous software developed for G4 can be used on putative iM searching and can calculate a  
383 numeric value to estimate iM (8,14,22) but there was no iM-specific experimental results which  
384 were fed into models to help with model design and training. In this paper, we developed both

385 a putative iM-forming sequence searching tool, Putative-iM-Searcher, and a machine learning  
386 approach to prediction of DNA iM folding status and folding strength, iM-Seeker. We  
387 considered that the identification of putative iM forming sequences, their folding status and  
388 folding strength were three significant parts of iM investigation that could benefit from  
389 computational predictions. Putative-iM-Searcher can construct directed graphs based on  
390 different configurations, can search all putative iM formations and conformations by graph  
391 traversal from input DNA sequences. Users can choose to set parameters including C-tract  
392 length, the first loop length, the second loop length, and the third loop length. The  
393 representative conformations can be obtained based on overlapping & non-overlapping  
394 strategy, greedy & non-greedy strategy, and representative-conformation strategy. Users can  
395 choose to obtain all putative iM formations and conformations as well. Based on the detected  
396 putative iMs by Putative-iM-Searcher, we used genome-wide CUT&Tag sequencing data and  
397 experimental data with pH<sub>T</sub> from previous studies and our experiments to develop iM-Seeker.  
398 This is the first time a machine learning approach has been applied to classification of this  
399 specific DNA structure motif and will significantly improve the accuracy of *in silico* iM prediction.  
400 The iMab antibody-based CUT&Tag sequencing data presents the folding status of C-rich  
401 sequences and iM-Seeker captures the difference between features in both folded iMs and  
402 unfolded C-rich sequences and allows for classification. Another regression model was trained  
403 on iM sequences derived from biophysical data, corresponding sequence with pH<sub>T</sub> to measure  
404 the folding strength.

405 iM-Seeker has good performance on both classification and regression tasks. The Balanced  
406 Random Forest classifier has higher performance in the imbalanced dataset. The number of  
407 folded iMs (8,837 iMs) is much less than unfolded motifs (733,115 iMs), which can mislead the  
408 classifier to overfit the unfolded dataset and classify folded iMs into unfolded category  
409 incorrectly. However, Balanced Random Forest is a decision-tree-based ensemble learning  
410 model that employs an under-sampling strategy to avoid overfitting of unfolded samples.  
411 Therefore, both folded samples and unfolded samples have good performance (recall 77%;  
412 specificity 81%). XGBoost, another ensemble learning approach which was also used in the G4  
413 classification mission (18), is selected for the estimation of folding strength among thirteen  
414 regressors. Although the number of data items for the regression model is limited, the  
415 regression part of iM-Seeker can also provide a reliable reference to evaluate the iM strength

416 (R<sup>2</sup> 0.642; RMSE 0.104; MAE 0.08). Previous studies investigated the iM formation features  
417 which can influence the iM strength by biophysical characterisation. The length of C-tracts,  
418 short loop length and high density of C and T can enhance the formation of iMs because other  
419 strong structures can be formed with G and A, which can result in the competition between  
420 iM and other structure motifs (8,55,56,61,62). Important features extracted from the regression  
421 model revealed a consistent result with previous research, which also justifies the reliability of  
422 our model. However, the stabilising effect of additional thymines is now quite well  
423 documented and consistent with the results observed here (29,63). Also the competition  
424 between guanines and cytosines were previously used in G4-hunter (14) as a scoring factor as  
425 having the complementary base within the sequences can skew structure formation towards  
426 hairpin (29).

427

428 iM-Seeker offers users the opportunity for a dedicated iM-searching tool, which is based on  
429 machine learning from existing datasets. The approach could be applied to other DNA and  
430 RNA structures where there is a wide range of data available, for example to further increase  
431 the accuracy of prediction of formation of G4 structures.

## 432 **SUPPLEMENTARY DATA**

433 Supplementary Data are available at NAR online.

434

## 435 **ACKNOWLEDGEMENT**

436 This research was partly supported by the Norwich Bioscience Institutes Partnership's Computing  
437 infrastructure for Science (CiS) group through the provision of a High-Performance Computing Cluster  
438 and the John Innes Centre Informatics team.

439

## 440 **FUNDING**

441 This work was supported by the United Kingdom Biotechnology and Biological Sciences Research  
442 Council (BBSRC) [BB/X01102X/1] (BY, HY, YD); [BB/W000962/1] (DG, ZW, YD); BBSRC Norwich Research  
443 Park Biosciences Doctoral Training Partnership [2578674] (BY); European Research Council (ERC)  
444 [selected by the ERC, funded by BBSRC Horizon Europe Guarantee [EP/Y009886/1] (YD); Human Frontier  
445 Science Program Fellowship [LT001077/2021-L] (HY);

446

447 **CONFLICT OF INTEREST**

448 The authors declare no competing financial interest.

449

450

451 **REFERENCES**

452

- 453 1. Lane, A.N., Chaires, J.B., Gray, R.D. and Trent, J.O. (2008) Stability and kinetics of G-quadruplex  
454 structures. *Nucleic acids research*, **36**, 5482-5515.
- 455 2. Gehring, K., Leroy, J.-L. and Guéron, M. (1993) A tetrmeric DNA structure with protonated  
456 cytosine-cytosine base pairs. *Nature*, **363**, 561-565.
- 457 3. Kang, C., Berger, I., Lockshin, C., Ratliff, R., Moyzis, R. and Rich, A. (1994) Crystal structure of  
458 intercalated four-stranded d (C3T) at 1.4 Å resolution. *Proceedings of the National Academy of  
459 Sciences*, **91**, 11636-11640.
- 460 4. King, J.J., Irving, K.L., Evans, C.W., Chikhale, R.V., Becker, R., Morris, C.J., Peña Martinez, C.D.,  
461 Schofield, P., Christ, D. and Hurley, L.H. (2020) DNA G-quadruplex and i-motif structure  
462 formation is interdependent in human cells. *Journal of the American Chemical Society*, **142**,  
463 20600-20604.
- 464 5. Zeraati, M., Langley, D.B., Schofield, P., Moye, A.L., Rouet, R., Hughes, W.E., Bryan, T.M., Dinger,  
465 M.E. and Christ, D. (2018) I-motif DNA structures are formed in the nuclei of human cells.  
466 *Nature chemistry*, **10**, 631-637.
- 467 6. Ma, X., Feng, Y., Yang, Y., Li, X., Shi, Y., Tao, S., Cheng, X., Huang, J., Wang, X.-e. and Chen, C.  
468 (2022) Genome-wide characterization of i-motifs and their potential roles in the stability and  
469 evolution of transposable elements in rice. *Nucleic Acids Research*, **50**, 3226-3238.
- 470 7. Zanin, I., Ruggiero, E., Nicoletto, G., Lago, S., Maurizio, I., Gallina, I. and Richter, S.N. (2023)  
471 Genome-wide mapping of i-motifs reveals their association with transcription regulation in  
472 live human cells. *Nucleic Acids Research*, **51**, 8309-8321.
- 473 8. Wright, E.P., Huppert, J.L. and Waller, Z.A. (2017) Identification of multiple genomic DNA  
474 sequences which form i-motif structures at neutral pH. *Nucleic acids research*, **45**, 2951-2959.
- 475 9. Huppert, J.L. and Balasubramanian, S. (2005) Prevalence of quadruplexes in the human  
476 genome. *Nucleic acids research*, **33**, 2908-2916.
- 477 10. Todd, A.K., Johnston, M. and Neidle, S. (2005) Highly prevalent putative quadruplex sequence  
478 motifs in human DNA. *Nucleic acids research*, **33**, 2901-2907.
- 479 11. Kudlicki, A.S. (2016) G-quadruplexes involving both strands of genomic DNA are highly  
480 abundant and colocalize with functional sites in the human genome. *PLoS One*, **11**, e0146174.
- 481 12. Kikin, O., D'Antonio, L. and Bagga, P.S. (2006) QGRS Mapper: a web-based server for predicting  
482 G-quadruplexes in nucleotide sequences. *Nucleic acids research*, **34**, W676-W682.
- 483 13. Eddy, J. and Maizels, N. (2006) Gene function correlates with potential for G4 DNA formation  
484 in the human genome. *Nucleic acids research*, **34**, 3887-3896.
- 485 14. Bedrat, A., Lacroix, L. and Mergny, J.-L. (2016) Re-evaluation of G-quadruplex propensity with  
486 G4Hunter. *Nucleic acids research*, **44**, 1746-1759.
- 487 15. Puig Lombardi, E. and Londoño-Vallejo, A. (2020) A guide to computational methods for G-  
488 quadruplex prediction. *Nucleic acids research*, **48**, 1-15.
- 489 16. Elimelech-Zohar, K. and Orenstein, Y. (2023) An overview on nucleic-acid G-quadruplex  
490 prediction: from rule-based methods to deep neural networks. *Briefings in Bioinformatics*, **24**,  
491 bbad252.
- 492 17. Hon, J., Martínek, T., Zendulka, J. and Lexa, M. (2017) pqsfinder: an exhaustive and  
493 imperfection-tolerant search tool for potential quadruplex-forming sequences in R.  
494 *Bioinformatics*, **33**, 3373-3379.
- 495 18. Cagirici, H.B., Budak, H. and Sen, T.Z. (2022) G4Boost: a machine learning-based tool for  
496 quadruplex identification and stability prediction. *BMC bioinformatics*, **23**, 1-18.

497 19. Sahakyan, A.B., Chambers, V.S., Marsico, G., Santner, T., Di Antonio, M. and Balasubramanian, 498 S. (2017) Machine learning model for sequence-driven DNA G-quadruplex formation. *Scientific 499 reports*, **7**, 14535.

500 20. Rocher, V., Genais, M., Nassereddine, E. and Mourad, R. (2021) DeepG4: a deep learning 501 approach to predict cell-type specific active G-quadruplex regions. *PLOS Computational 502 Biology*, **17**, e1009308.

503 21. Lorenz, R., Bernhart, S.H., Höner zu Siederdissen, C., Tafer, H., Flamm, C., Stadler, P.F. and 504 Hofacker, I.L. (2011) ViennaRNA Package 2.0. *Algorithms for molecular biology*, **6**, 1-14.

505 22. Belmonte-Reche, E. and Morales, J.C. (2020) G4-iM Grinder: when size and frequency matter. 506 G-Quadruplex, i-Motif and higher order structure search and analysis tool. *NAR genomics and 507 bioinformatics*, **2**, lqz005.

508 23. Mergny, J.L. and Lacroix, L. (2009) UV melting of G - quadruplexes. *Current protocols in nucleic 509 acid chemistry*, **37**, 17.11. 11-17.11. 15.

510 24. Mergny, J.-L., Li, J., Lacroix, L., Amrane, S. and Chaires, J.B. (2005) Thermal difference spectra: 511 a specific signature for nucleic acid structures. *Nucleic acids research*, **33**, e138-e138.

512 25. Iaccarino, N., Di Porzio, A., Amato, J., Pagano, B., Brancaccio, D., Novellino, E., Leardi, R. and 513 Randazzo, A. (2019) Assessing the influence of pH and cationic strength on i-motif DNA 514 structure. *Analytical and bioanalytical chemistry*, **411**, 7473-7479.

515 26. Nguyen, T., Fraire, C. and Sheardy, R.D. (2017) Linking pH, temperature, and K<sup>+</sup> concentration 516 for DNA i-Motif formation. *The Journal of Physical Chemistry B*, **121**, 7872-7877.

517 27. Gurung, S.P., Schwarz, C., Hall, J.P., Cardin, C.J. and Brazier, J.A. (2015) The importance of loop 518 length on the stability of i-motif structures. *Chemical Communications*, **51**, 5630-5632.

519 28. Meers, M.P., Tenenbaum, D. and Henikoff, S. (2019) Peak calling by Sparse Enrichment Analysis 520 for CUT&RUN chromatin profiling. *Epigenetics & chromatin*, **12**, 1-11.

521 29. Guneri, D., Alexandrou, E., El Omari, K., Dvorakova, Z., Chikhale, R.V., Pike, D., Waudby, C.A., 522 Morris, C.J., Haider, S. and Parkinson, G.N. (2023) Structural Insights into Regulation of Insulin 523 Expression Involving i-Motif DNA Structures in the Insulin-Linked Polymorphic Region. *bioRxiv*, 524 2023.2006. 2001.543149.

525 30. Williams, S.L., Casas-Delucchi, C.S., Raguseo, F., Guneri, D., Li, Y., Minamino, M., Fletcher, E.E., 526 Yeeles, J.T., Keyser, U.F., Waller, Z.A. *et al.* (2023) Replication-induced DNA secondary structures 527 drive fork uncoupling and breakage. *The EMBO Journal*, **42**, e114334.

528 31. Dhapola, P. and Chowdhury, S. (2016) QuadBase2: web server for multiplexed guanine 529 quadruplex mining and visualization. *Nucleic acids research*, **44**, W277-W283.

530 32. Kingsford, C. and Salzberg, S.L. (2008) What are decision trees? *Nature biotechnology*, **26**, 531 1011-1013.

532 33. Breiman, L. (2001) Random forests. *Machine learning*, **45**, 5-32.

533 34. Chen, C., Liaw, A. and Breiman, L. (2004) Using random forest to learn imbalanced data. 534 *University of California, Berkeley*, **110**, 24.

535 35. Webb, G.I., Keogh, E. and Miikkulainen, R. (2010) Naïve Bayes. *Encyclopedia of machine 536 learning*, **15**, 713-714.

537 36. Balakrishnama, S. and Ganapathiraju, A. (1998) Linear discriminant analysis-a brief tutorial. 538 *Institute for Signal and information Processing*, **18**, 1-8.

539 37. Liu, X.-Y., Wu, J. and Zhou, Z.-H. (2008) Exploratory undersampling for class-imbalance learning. 540 *IEEE Transactions on Systems, Man, and Cybernetics, Part B (Cybernetics)*, **39**, 539-550.

541 38. Maclin, R. and Opitz, D. (1997) An empirical evaluation of bagging and boosting. *AAAI/IAAI*, 542 **1997**, 546-551.

543 39. Hido, S., Kashima, H. and Takahashi, Y. (2009) Roughly balanced bagging for imbalanced data. 544 *Statistical Analysis and Data Mining: The ASA Data Science Journal*, **2**, 412-426.

545 40. Seiffert, C., Khoshgoftaar, T.M., Van Hulse, J. and Napolitano, A. (2009) RUSBoost: A hybrid 546 approach to alleviating class imbalance. *IEEE transactions on systems, man, and cybernetics- 547 part A: systems and humans*, **40**, 185-197.

548 41. Chen, T. and Guestrin, C. (2016) *Proceedings of the 22nd ACM SIGKDD international conference*  
549 *on knowledge discovery and data mining*, pp. 785-794.

550 42. Su, X., Yan, X. and Tsai, C.L. (2012) Linear regression. *Wiley Interdisciplinary Reviews: Computational Statistics*, **4**, 275-294.

552 43. McDonald, G.C. (2009) Ridge regression. *Wiley Interdisciplinary Reviews: Computational Statistics*, **1**, 93-100.

554 44. Tibshirani, R. (1996) Regression shrinkage and selection via the lasso. *Journal of the Royal Statistical Society Series B: Statistical Methodology*, **58**, 267-288.

556 45. Zou, H. and Hastie, T. (2005) Regularization and variable selection via the elastic net. *Journal of the Royal Statistical Society Series B: Statistical Methodology*, **67**, 301-320.

558 46. Awad, M., Khanna, R., Awad, M. and Khanna, R. (2015) Support vector regression. *Efficient learning machines: Theories, concepts, and applications for engineers and system designers*, 67-80.

560 47. Wang, J., Chen, Q. and Chen, Y. (2004) *International symposium on neural networks*. Springer, pp. 512-517.

562 48. Altman, N.S. (1992) An introduction to kernel and nearest-neighbor nonparametric regression. *The American Statistician*, **46**, 175-185.

564 49. Freund, Y. and Schapire, R.E. (1997) A decision-theoretic generalization of on-line learning and an application to boosting. *Journal of computer and system sciences*, **55**, 119-139.

566 50. Friedman, J.H. (2001) Greedy function approximation: a gradient boosting machine. *Annals of statistics*, 1189-1232.

568 51. Fischler, M.A. and Bolles, R.C. (1981) Random sample consensus: a paradigm for model fitting with applications to image analysis and automated cartography. *Communications of the ACM*, **24**, 381-395.

570 52. Pedregosa, F., Varoquaux, G., Gramfort, A., Michel, V., Thirion, B., Grisel, O., Blondel, M., Prettenhofer, P., Weiss, R. and Dubourg, V. (2011) Scikit-learn: Machine learning in Python. *the Journal of machine Learning research*, **12**, 2825-2830.

572 53. Lemaître, G., Nogueira, F. and Aridas, C.K. (2017) Imbalanced-learn: A python toolbox to tackle the curse of imbalanced datasets in machine learning. *The Journal of Machine Learning Research*, **18**, 559-563.

574 54. Wright, E.P., Abdelhamid, M.A., Ehiabor, M.O., Grigg, M.C., Irving, K., Smith, N.M. and Waller, Z.A.E. (2020) Epigenetic modification of cytosines fine tunes the stability of i-motif DNA. *Nucleic Acids Research*, **48**, 55-62.

576 55. Fojtík, P. and Vorlíčková, M. (2001) The fragile X chromosome (GCC) repeat folds into a DNA tetraplex at neutral pH. *Nucleic Acids Research*, **29**, 4684-4690.

578 56. Fleming, A.M., Ding, Y., Rogers, R.A., Zhu, J., Zhu, J., Burton, A.D., Carlisle, C.B. and Burrows, C.J. (2017) 4 n - 1 is a “sweet spot” in DNA i-motif folding of 2' -deoxycytidine homopolymers. *Journal of the American Chemical Society*, **139**, 4682-4689.

580 57. Brazier, J.A., Shah, A. and Brown, G.D. (2012) I-motif formation in gene promoters: unusually stable formation in sequences complementary to known G-quadruplexes. *Chemical Communications*, **48**, 10739-10741.

582 58. Mir, B., Serrano, I., Buitrago, D., Orozco, M., Escaya, N. and González, C. (2017) Prevalent sequences in the human genome can form mini i-motif structures at physiological pH. *Journal of the American Chemical Society*, **139**, 13985-13988.

584 59. Abdelhamid, M.A. and Waller, Z.A. (2020) Tricky topology: persistence of folded human telomeric i-motif DNA at ambient temperature and neutral pH. *Frontiers in Chemistry*, **8**, 40.

586 60. Martella, M., Pichiorri, F., Chikhale, R.V., Abdelhamid, M.A., Waller, Z.A. and Smith, S.S. (2022) i-Motif formation and spontaneous deletions in human cells. *Nucleic Acids Research*, **50**, 3445-3455.

588 61. Brooks, T.A., Kendrick, S. and Hurley, L. (2010) Making sense of G - quadruplex and i - motif functions in oncogene promoters. *The FEBS Journal*, **277**, 3459-3469.

599 62. Abou Assi, H., Garavís, M., González, C. and Damha, M.J. (2018) i-Motif DNA: structural  
600 features and significance to cell biology. *Nucleic acids research*, **46**, 8038-8056.  
601 63. Yazdani, K., Seshadri, S., Tillo, D., Yang, M., Sibley, C.D., Vinson, C. and Schneekloth Jr, J.S. (2023)  
602 Decoding complexity in biomolecular recognition of DNA i-motifs with microarrays. *Nucleic  
603 Acids Research*, gkad981.  
604